Processing of metals and dielectric materials with ps-laserpulses: results, strategies, limitations and needs

Beat Neuenschwander*, Guido F. Bucher, Christian Nussbaum, Benjamin Joss,
Martin Muralt, Urs W. Hunziker Peter Schuetz
Bern University of Applied Sciences Engineering and Information Technologies,
Pestalozzistrasse 20, CH-3400 Burgdorf, Switzerland

ABSTRACT

Ultra short (ps, fs) laser pulses are used, when high requirements concerning accuracy, surface roughness, heat affected zone etc. are demanded for surface structuring. Ps-laser systems that are suited to be operated in industrial environments are of great interest for many practical applications. Here results in the field of 3-d structuring (metals and transparent materials), induced processes and structuring of flexible solar cells will be presented.
Beside the pulse duration, which is given by the laser system, the user has a wide variety of optimization parameters such as fluence, repetition rate and wavelength. Based on a simple model it will be shown, that there exist optimum laser parameters to achieve maximum volume ablation rates at a given average power. To take benefit of these optimum parameters and to prevent harmful effects like plasma shielding and surface melting, adapted structuring strategies, depending on the requirements, have to be used. Today's ultra short pulsed systems have average powers from a few W up to a few 10W at high repetition rates. The actual available beam guiding systems are limited and can often not fulfill the requirements needed for high throughput structuring with optimized parameters. Based on the achieved results, the needs for future beam guiding systems will be discussed.

Keywords: Laser micro machining, ultra short pulses, ps-laserpulses, ablation model, process optimization

1. INTRODUCTION

With the availability of industrially suited ultra short pulsed laser systems with pulse energies from a few µJ up to a few 100 µJ at repetition rates of some 10 kHz up to MHz the interest in using these pulses for micro material processing has strongly increased also in the industrial field. Compared to ns-pulses from Q-switched systems, ultra short pulses show less negative thermal effects due to the significantly reduced thermal penetration depth. Furthermore, in the case of isolators, one can benefit from increased nonlinear effects as for example multi-photon absorption or frequency conversion, which are nearly absent for ns-pulses. In metals the absorption process is described with the two temperature model[1], where the temperatures of the free electrons which are absorbing the energy of the laser pulse and the lattice are treated separately. The time for the energy transfer from the free electrons to the lattice, the electron-phonon thermalization time, amounts a few ps[2,3]. A further reduction of the pulse duration will not lead to additional benefits in terms of the material response, rather it can lead to a reduced precision and to increased unwanted plasma effects[2,3]. For metals therefore the optimal pulse duration for obtaining highest precision amounts a few ps. As ps-systems are mostly set up as master oscillator post amplifier (MOPA) systems without pulse stretcher and compressor they can be built very stable also at high power. They were therefore the first ultra short pulsed systems entering into the field of industrial micro material processing. In many cases ps-systems can also be used for the processing of different dielectric materials and semiconductors. Beside all these advantages one has also to obtain a high throughput to be competitive to other laser systems or alternative technologies. This was one of the reasons to develop ps-systems with average powers up to 50W[4,5]. To really take benefit of these high average powers, one has to optimize the whole chain from the laser parameters over the beam guiding system to the process and the process strategies.

*beat.neuenschwander@bfh.ch; phone +41 34 426 42 20; fax +41 34 423 15 13; ti.bfh.ch

2. APPLICATIONS WITH TRANSPARENT MATERIALS

The transparent materials sapphire, borosilicate glass and lithium niobate $LiNbO_3$ serve as examples for isolators. All experiments were performed with a DUETTO[4] ps-lasersystem. This system generates pulses with a duration of about 10ps at an average power of about 10W. The repetition rate can be varied between 50kHz and 1MHz and the beam quality is $M^2<1.3$. A second special amplifier box contains an electro optic modulator which works from 50kH to 300kHz repetition rate. Whit this pulse picker the repetition rate can be further reduced down to single shot and the beam can be switched on and off. With an additional booster amplifier in this box the pulse energy can be raised up 600µJ at a repetition rate of 1kHz. The fundamental wavelength amounts 1064nm and can be doubled to 532nm or tripled to 355nm. For each wavelength the beam is guided to a separate galvo-scanner (Turboscan and Superscan from Raylase). By using different telecentric or f-θ objectives the spot achievable radius can be varied from 36µm to 7µm for 1064nm, from 22µm to 4µm for 532nm and from 10µm to 2µm for 355nm.

2.1 Engraving

3d laser inner engraving of glasses is well known since a few years. It has been first demonstrated 1971 by Agadjanov[6] and was significantly improved in the following years. The beam of a pulsed Q-switch system at a wavelength of 1064nm or 532nm is focused into the glass body. Above a certain intensity threshold, each focused laser pulse induces a dielectric breakdown resulting in a micro crack in the glass body. Typical dimensions of these cracks are a few 10µm in length and diameter. These micro cracks always go with mechanical stresses in the material. If the spacing between the single cracks is too small, a mechanical fracture between the single cracks arises and may propagate through the whole structure. The mechanical stresses therefore limit the spacing between the single cracks. Inner engraving can also be achieved very well with ps-laserpulses. Figure 1 shows the engraving of a logo in a sapphire watch glass with pulses of 10ps duration at a wavelength of 355nm and a spot radius of about 5µm. The single cracks are very narrow and the typical fracture observed for ns-pulses do not appear. Therefore very fine lines ore a complete area can be marked with these pulses.

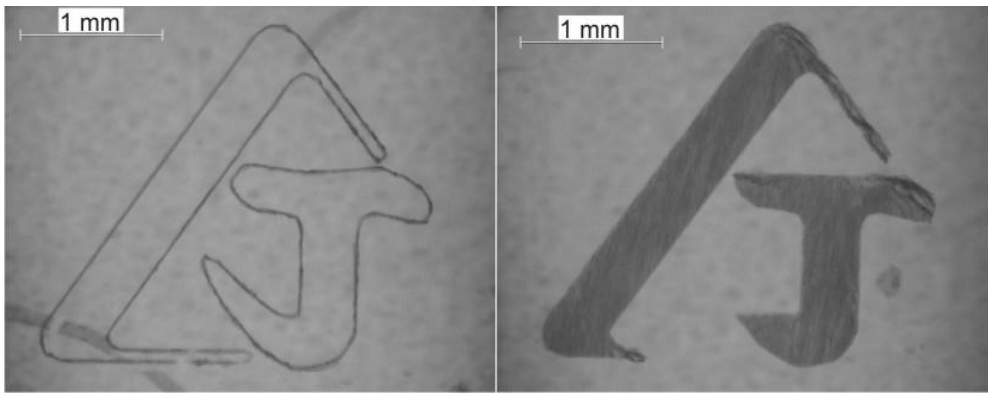

Figure 1: Inner engraving of a logo in sapphire watch glass with ps-laserpulses of 10ps pulse duration, 355nm wavelength and 5µm spot radius. The outline of the logo is shown on the left side whereas on the right side the filled logo is shown.

In contrast to inner engraving, marking on the surface is achieved by an ablation process. The laser beam is focused onto the surface of the target and guided via a galvo scanner. Compared to ns-pulses, a qualitatively good marking of sapphire, fused silica or borosilicate can be also achieved at 1064nm and 532nm wavelength. Due to the nonlinear Kerr-effect a self focusing of the pulses propagating through the transparent medium can appear. This has been observed with micro slides from borosilicate of 1mm thickness. When the 532nm beam is focused to a spot radius of 7-10µm on the front side of the slide the self focusing leads to an about 20% smaller ablation threshold on the back side. This allows the setting of the marked side of the slide by the pulse energy. An identical mark on both sides without turning the slide can be achieved in two runs by properly adjusting the pulse energy for each run, as shown in figure 2.

2.2 Drilling

Lithium niobate plates are used as waveguides for THz-waves. When these plates are covered with a special pattern of holes, they can act as a photonic crystal and the propagation of the THz wave can be influenced and controlled. A suitable hole diameter for this application amounts about 50µm. To deduce the best suited laser parameters an analysis of the threshold fluence was done for the three wavelengths 1064nm, 532nm and 355nm. To this end the beam was focused onto the surface of a lithium niobate plate, a Gaussian intensity distribution was assumed and the area of the ablated spot on the surface was deduced for different pulse energies. A logarithmic fit to the measured areas lead to the threshold fluences of 1.8J/cm^2 for 1064nm, 1.27J/cm^2 for 532nm and 0.64/cm^2 for 355nm as shown in figure 3.

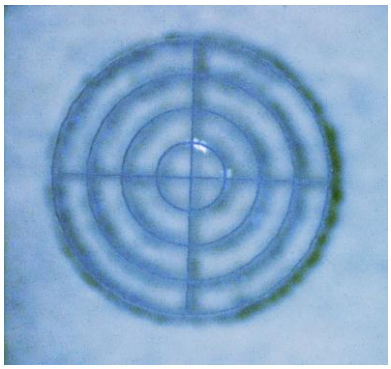

Figure 2: Identical butts marked on both sides of a micro slide. The back side, corresponding to the upper side in the picture, is marked with pulse energies between the threshold for front- and backside marking. The front side (backside in the picture) is marked with higher pulse energies. Due to the self focusing the lines on the backside are very fine. The frond side marking arises as a shadow in the picture.

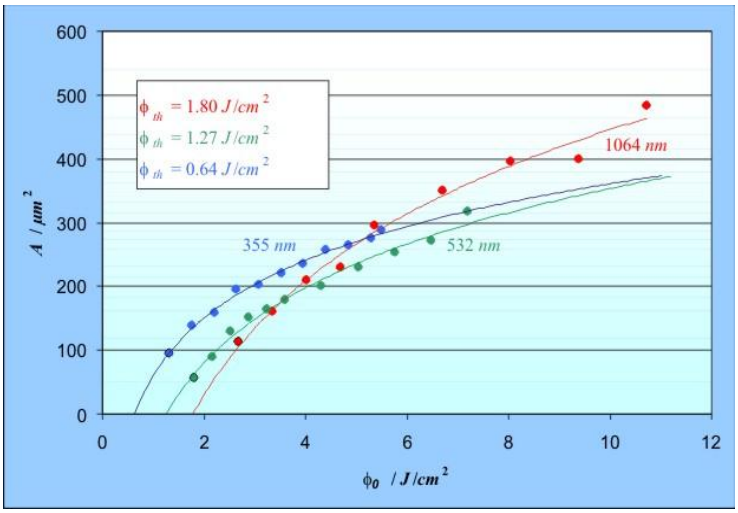

Figure 3: Ablated area as a function of the fluence for the three wavelengths 1064nm, 532nm and 355nm. The threshold fluence is determined by a logarithmic fit based on the assumption of a Gaussian intensity distribution.

Its lowest threshold and the highest Rayleigh range at a given spot size make 355nm to the preferable wavelength for the drilling process. The holes were helically drilled with a galvo scanner with a spot radius of 5µm and a trepanning radius of 30µm. One critical point is the damage of the surface at the entrance or the exit of the hole at too high pulse energies. Best results with minimum surface damages were achieved for a pulse energy of about 40µJ, a repetition rate of 1kHz and a trepanning frequency of 20Hz. Unfortunately these parameters always lead to conical holes with smaller diameters at the exit as shown in the left of figure 4 for a plate thickness of 500µm. Cylindrical holes are obtained in 250µm tick plates by drilling from both sides. In this case the plate has to be flipped over and exactly replaced after the first drilling process. The achieved result for a 50µm diameter hole is shown on the right in figure 4. To deduce the surface quality at the wall of the hole, a cut through a hole was analyzed under the laser scanning microscope as shown left in figure 5. The topographic information along a line (marked blue in figure 4) was evaluated and a maximum variation of 1.8µm and a

R_a-value of 0.19µm, corresponding to a N3 surface, was observed. No other strategy with varying pulse energies and trepanning parameters was found to achieve cylindrical holes by drilling from one side. This situation would of course change if a special drilling optics could be used.

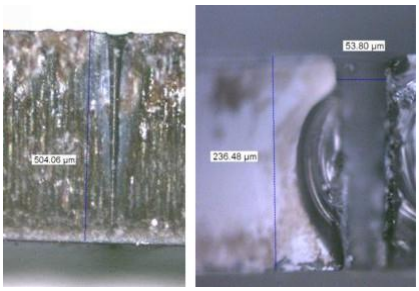

Figure 4: Drilled holes in lithium niobate. Left: A conical hole is obtained when the plate is drilled from one side only. Here the result of a 500µm thick plate is shown. Right: When the plate is flipped over, exactly replaced and drilled from both sides, the holes become cylindrical for a plate thickness of 250µm or smaller.

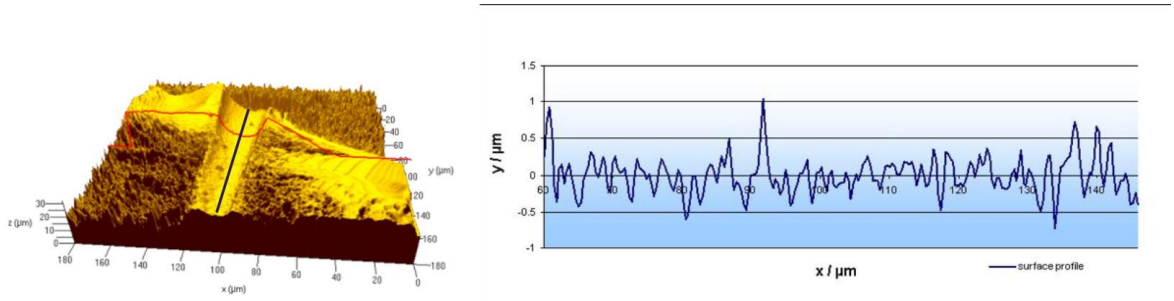

Figure 5: Left: Topography of the cut through a drilled hole measured with a laser scanning microscope. The topographic information along the blue parallel line through the hole is plotted in the right of the figure. The R_a-value amounts 0.19µm.

2.3 Surface structuring

For surface structuring a given outline is filled with rectangular crossed parallel lines. The distance between the lines can be varied but not fall below a certain value given by the driver software of the galvo-scanner and the focal length of the used scanner objective. The best suited fluence and pulse overlap are deduced with a parameter study by generating 1x1mm shaped squares with varying average power and marking speed at constant repetition rate. Figure 6 shows an example in borosilicate with 532nm wavelength. At high pulse energies and low marking speeds going with high average power and high pulse overlap very strong debris is observed. This debris may tower to a height bigger than the lateral dimension of the structure. The debris can‘t be completely removed with subsequent cleaning process in an ultrasonic bath or with cleaning tissues and acetone. In contrast, at low and moderate average power and high marking speed one observes local dropouts in the marking process. These dropouts indicate that the material removal process is a combination between an ablation process and mechanical spalling. Optimal results with minimal debris and low surface roughness are obtained at moderate average powers, going with pulse energies and fluences which are clearly but not by decades above the threshold, and higher but not maximal marking speeds.

These parameters are used to build up 3 dimensional structures in a 2½ dimensional process. The desired structure is divided into different slices from which the filled outline is marked with rectangular crossed parallel lines. The structure is then generated slice by slice into the material. For a high deepness of the structure, it becomes necessary to track the position of the focus by moving the target or adapting the beam divergence in front of the galvo scanner. Figure 7 shows a twisted pyramid and a special formed structure in sapphire as to examples of 3d structures produced at 355nm. The lateral dimension of both structures is 1.5mm and the deepness is 120µm for the pyramid and 80µm for the special formed structure. When the angle of the rectangular crossed parallel lines rests unchanged from slice to slice, a

pronounced corresponding pattern at the bottom of the structure is obtained. This pattern is averted by turning the angle of the rectangular crossed parallel lines from slice to slice. With this technology, also the surface roughness can be reduced compared to a fixed angle.

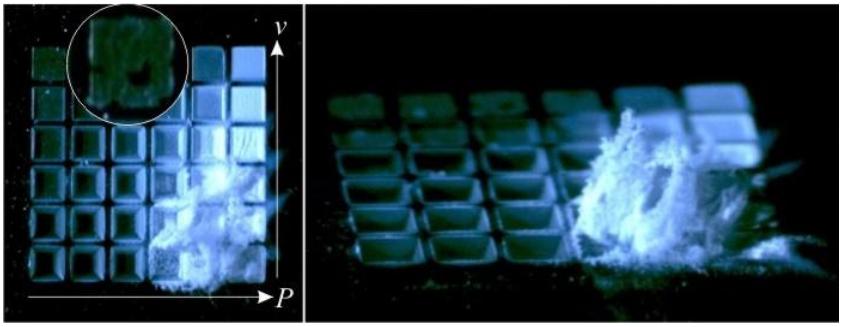

Figure 6: Parameter study in borosilicate. The matrix consists of 6x6 1mm sized squares. From Left to the right the average power is increased and from the bottom to the top the marking speed is raised. Strong debris is observed for high average power going with high pulse energy and low marking speed (high pulse overlaps). At moderate average power and high marking speeds (small pulse overlap) one observes dropouts in the ablation process as shown magnified in the top of the left picture.

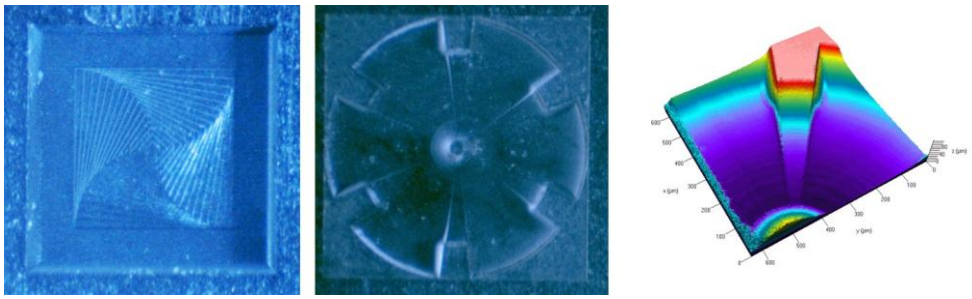

Figure 7: Twisted pyramid (left) and special formed structure (center and right) as examples for 3d structures in sapphire produced at 355nm wavelength. The lateral dimension of both structures is 1.5mm. The right picture shows the topography of the special formed structure measured with a laser scanning microscope.

2.4 Laser induced plasma assisted ablation

The laser induced plasma assisted ablation (LIPAA) process, shown in figure 8, was first used to produce microstructures in quartz and glass with ns laser pulses in the UV[7,8] and in the visible or NIR range[9,10]. Beside the possibility for a fine and precise ablation of the transparent substrate, the LIPAA process can also be used to coat or color the transparent substrate. Coloring and coating facilities were widely investigated with ns- and fs- laser pulses. In the case of metallic targets the generation of conducting paths and microstructures becomes possible; a good overview, also about the impact in microelectronics, is for example given in[11,12].

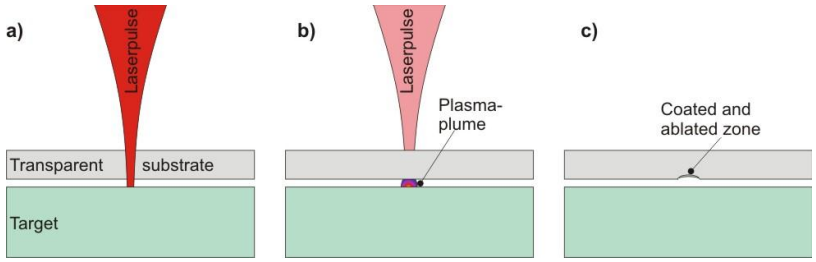

Figure 8: Scheme of the LIPAA process. a) A transparent substrate is placed on an opaque target, typically a metal. A laser pulse penetrates the substrate and is absorbed in the target. b) The absorbed laser radiation causes an expanding plasma plume. Depending on the laser pulse duration, the plasma plume itself may be influenced by the laser pulse c) The plasma plume leads to an ablated and coated zone on the transparent substrate.

Also ps-pulses are well suited for this application. The used experimental set-up is shown left in figure 9. The pulses from the Duetto ps-laser system are focused via a galvo scanner through the transparent substrate onto the target. Both (target and substrate) are placed in a process chamber which can be evacuated down to 50 mbar and flooded with a gas, e.g. argon. The distance between the target and the substrate is adjusted with a combination of spacers of 10, 20, 50 and 100µm thicknesses. As a typical result of the LIPAA process with ps-pulses chess boards generated with an aluminum target and eleven parallel conducting lines generated with a copper target are shown in the centre and in the right of figure 9. Both structures have been generated in a 50mbar argon atmosphere and a distance of 50µm between target and substrate.

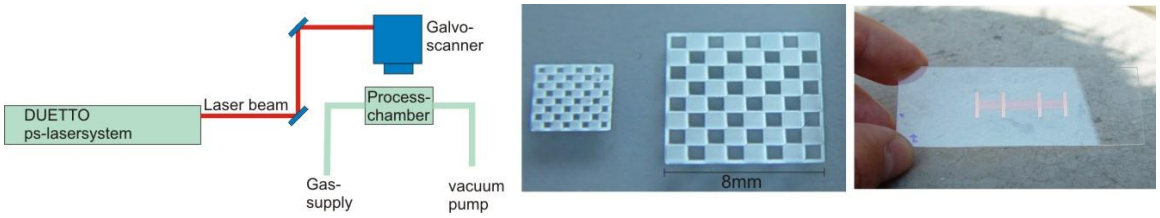

Figure 9: Left: Sketch of the experimental set up. Center: Chess boards with 4mm and 8mm side length, generated with aluminum as target in a 50mbar argon atmosphere. Right: Eleven parallel conducting lines with generated with copper as target. The slide is prepared for the four-probe sensing method.

The metallic brilliance implies that the structures are electrical conductive. With aluminum as target in 50µm distance to the substrate, a 50mbar argon atmosphere and at 532nm wavelength a parameter study was performed[13]. The results are shown in the left of figure 10. The highest line conductance of 500S*µm was achieved at an average power of 125mW, a marking speed of 3mm/s with 20µm spot diameter and 50kHz repetition rate. The written lines become broader than the spot size and consist of deposited sub-µm particles. The average grain size, the area covered with particles and the number of particles per area exponentially drop with the lateral distance to the center of the marked line. When parallel lines are generated, the specific line conductance becomes dependent of the line spacing due to a possible cross talk[13]. In the right of figure 10 the specific line conductance of eleven parallel copper lines for two distances between substrate and target are shown and compared with a model basing on the exponential drop of the average grain size and the covered area with particles.

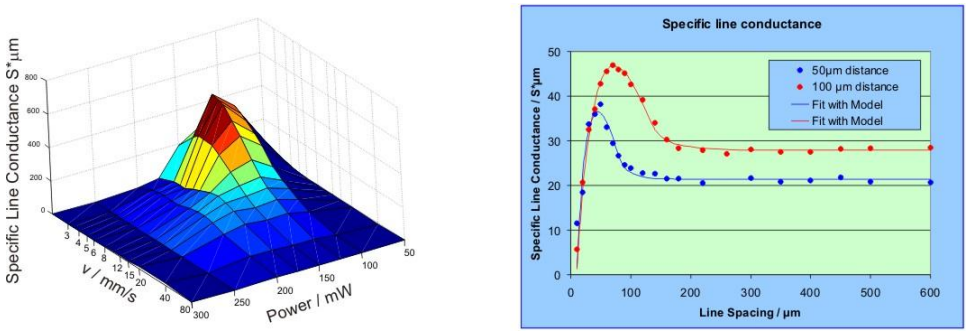

Figure 10: Left: Specific line conductance for lines generated with a 20µm diameter spot at 532nm in a 50mbar argon atmosphere for different average powers and marking speeds. The repetition was set to 50kHz and the distance between target and substrate amounted 50µm. Right: Specific line conductance of eleven parallel copper lines as a function of its spacing. The analytical model used for the fit bases on the assumption of a perpendicular exponential drop of the average grain size and the covered area of the deposited sub-µm particles.

3. APPLICATIONS WITH SEMICONDUCTORS

Drilling and structuring of crystalline or amorphous semiconductors is also possible in the same way as presented in the previous sections. A very interesting application is the removal of thin amorphous semiconductor films or in general the removal of thin films for flexible and thin film solar cells. In this case one often speaks from the P1-, the P2- and P3-scribe[14]. ps-laser pulses are well suited for all three scribes, but depending on the used material for the cells, sometimes with different wavelengths for the single scribes. An example for a P3-scribe into a CIGS solar cell is shown in figure

11. The SEM image and the EDX analysis shows that in the scribe the zinc oxide layer is removed down to the CIGS layer which seems to be nearly unaffected.

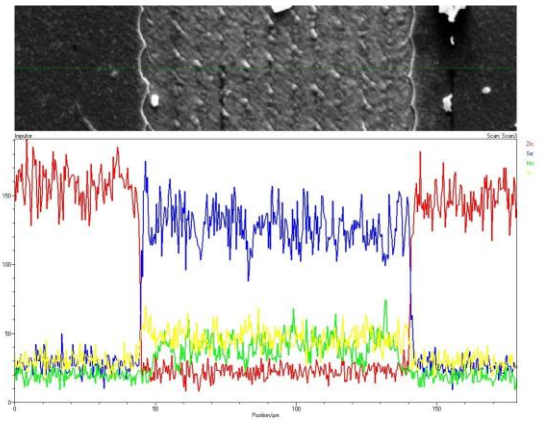

Figure 11: SEM image and EDX analysis of a P3 scribe into a flexible CIGS solar cell. The red line denotes the element zinc, the blue line selenium, the green line molybdenum and the yellow line indium. In the scribe the amount of zinc almost vanishes whereas the amount of selenium drastically increases. Also the amount of indium, which is also part of the CIGS layer, increases in the scribe. The higher amount of molybdenum which forms the conducting layer beyond the CIGS layer indicates that the electrons from the EDX analysis penetrate through the CIGS layer.

For the P1-scribe one found during the last years, that a back-scribing process shows many advantages[15,16]. In the back-scribing process the laser radiation is focused through the transparent substrate material onto the layer which is removed. Considering the energy balance leads to the recognition that this process is from non-thermodynamic nature[16], which also explains the improved results at the border of the scribe.

4. APPLICATIONS WITH METALS

Laser micro processing of metals with short and ultra short pulses was intensively investigated during the last decade and represents one of the most promising fields for the need of ps-laser pulses. In metals, the thermal penetration depth ℓ_{th} mostly dominates the optical one for ps or longer laserpulses. This penetration depth depends from the square of the pulse duration $\Delta\tau$ and the thermal diffusivity κ.

$$\ell_{th} = 2 \cdot \sqrt{\kappa \cdot \Delta\tau} \qquad (1)$$

This quite simple expression holds for pulse duration down to about 10ps, for shorter pulse durations this penetration depth almost remains constant[2,3]. As the thickness of the heat affected zone (HAZ) is in the range of the thermal penetration depth a further reduction of the pulse duration does not make sense with respect to the accuracy. Furthermore the pulse duration of a few ps also prevents from unwanted plasma effects and allows the use of simpler and therefore cheaper laser systems than with fs-pulses. Very interesting applications are high precision drilling, 3d-structuring of surfaces and high quality cutting of thin blanks and sheets. In figure 12 examples for cutting and structuring are shown. The cutting edges are clean without thermal damages on the surface. In the middle a mounted T-Rex from 50µm thick steal foils is shown. The size limitation is at the moment not given by the possibility of high precise cutting of smaller foils but by the possibility of assembling the single parts with the tweezers. The author wishes to thank his assistant for the six hour assembly work for the present T-Rex.

On the right side of figure 12 a 3d-surface structure, the topography of Switzerland in copper, generated with the technology presented in section 2.3 is shown. The darker look of the mountains (the Alps) is not due to a coloring like oxidation in the copper but due to the different reflection of the illumination light at oblique surfaces. In general the copper surface rests very brilliant and absolutely no oxidation of this surface can be observed at suitable laser parameters. For this example 532nm ps-pulses with an average power of about 400mW, a repetition rate of 300kHz, a marking speed of 300mm/s and a spot radius of about 7µm were used. The topography is divided into 100 slices and the outline of each slice was filled with parallel (not rectangular crossed parallel) lines with a distance of 9µm. The minimum line distance of this filling pattern was limited by the scanner software and could not be further decreased. The

angle sequence of the filling pattern was 0°, -90°, 45°, -45°, 5°, -85°, 50°, -40°, … . When the average power was enlarged or the marking speed was decreased, the copper surface began to oxidate. In contrast to drilling where high pulse energies are first used to eject the material from the hole, cutting of thin sheets and 3d-structuring show much better and accurate results at low pulse energies and higher repetition rates. As always a part of the pulse energy is still converted to heat, one has to ensure that this thermal energy is not locally damming up and therefore the beam has to be moved with appropriate speeds, i.e. 300mm/s for the presented example in figure 12.

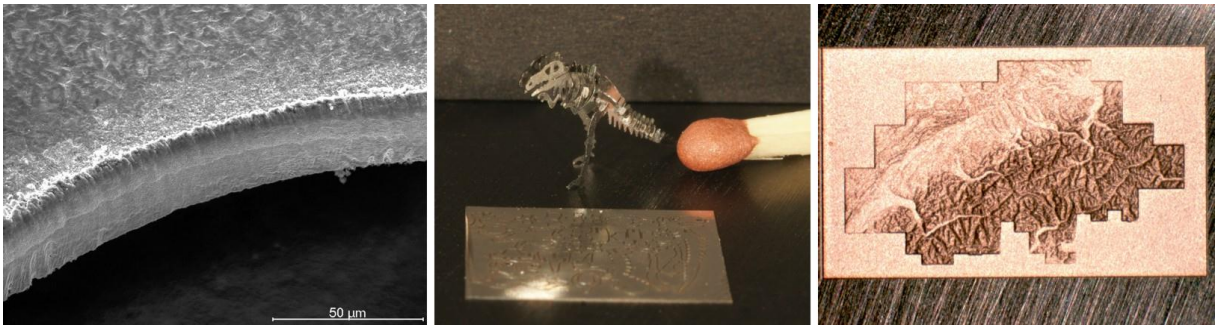

Figure 12: Examples for metal processing with ps-pulses. Right: Big hole in a thin steal foil. Center: Self assembly kit and mounted T-Rex cut in 50µm thick steal foil. Right: Topography of Switzerland in a copper blank. The dimensions are about 10x6mm and 80µm depth only cleaned with acetone and lens cleaning paper. The metallic brilliance shows that now oxidation process has appeared.

A decrease in the process time can therefore only be achieved by scaling up the average power together with the repetition rate to keep the pulse energy and the fluence constant. Also the overlap from pulse should at least be constant or eventually enlarged to keep the local average intensity quite small. And therefore the marking speed scales at least with the average power. In the present example this means, that for an average power of 4W, the repetition rate has to be 3MHz and the marking speed 3000mm/s and this with unchanged accuracy. This simple calculation shows, that today scanner systems will be at its limit even for moderate average powers of a few Watts. A very interesting possibility to decrease the process speed by enlarging the process efficiency is the use of pulse bursts which works for ns-pulses[17] as well as for ps-pulses[18,19] where an increase of the ablation rate of several 10% has been observed.

For many practical applications as e.g. printing industries[20] also structures with lateral dimensions in the range of 100µm are of great interest. Figure 13 shows as an example 100µm side length positive and negative shaped pyramid in copper. Due to the limited accuracy the generation of these structures is almost impossible with common galvo-scanners. Furthermore, due to assimilated heat it will not be possible to generate such a single structure with 100µm lateral dimension with an average power on the range of a few Watts. To prevent from overheating the average power has to be distributed over an adequate surface area i.e. multiple structures have to be generated in one work item.

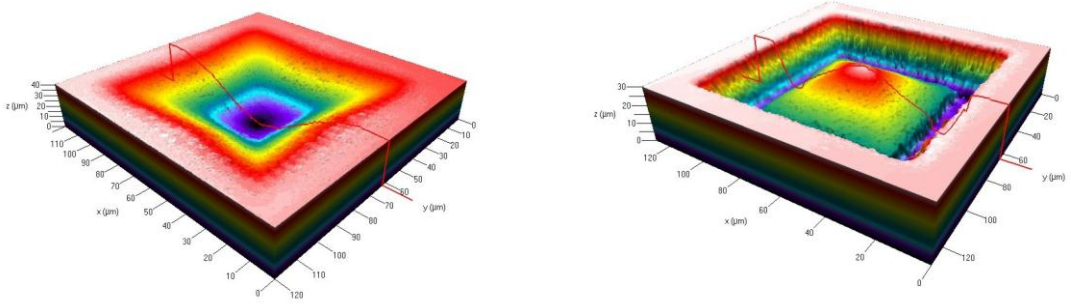

Figure 13: Negative (right) and positive (left) shaped pyramid with 100µm side length in copper.

The pyramids in figure 13 were generated with two crossed linear stages. The stages stopped always at the desired position and one pulse was fired onto the target. The pyramids were also built up slice by slice. With this of course slow method, many different structuring strategies can be easily tested. A strategy which allows the generation of such small

structures with small surface roughness is illustrated in figure 14. One slice consists of several layers. In one layer single pulses are concatenated in the distance of about one spot diameter. From layer to layer the pattern is shifted in a defined sequence. With such strategies a surface roughness of less than 300nm can be achieved also in the walls of the structure.

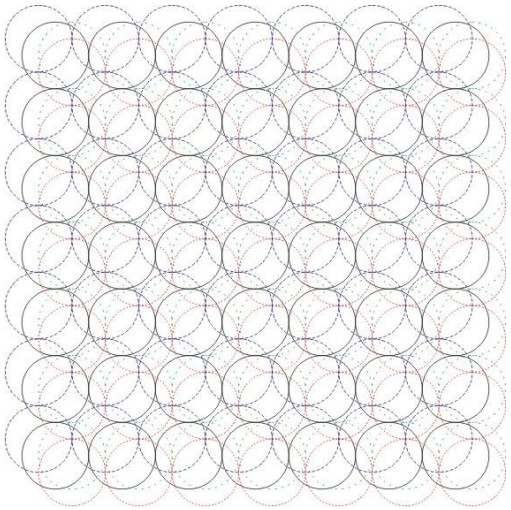

Figure 14: A possible strategy to generate small pyramids. Each slice is divided into several layers. In one layer the pulses are concatenated in the distance of the spot radius.

The full access and control over the instant position of the laser beam is needed to implement such strategies. In conclusion that implies that the laser system itself is the clock for the regulation and control of the beam guiding system.

5. A MODEL FOR OPTIMIZED PROCESS EFFICIENCY

5.1 Ablation model for short and ultra short pulses

It is often reported in literature[21,22], that for short and ultra short pulses the ablation depth z_{abl} logarithmically depends on the laser fluence ϕ:

$$z_{abl} = \delta \cdot \ln\left(\frac{\phi}{\phi_{th}}\right) \tag{2}$$

Where δ is some kind of penetration depth and ϕ_{th} denotes the threshold fluence. In the case of ultra short pulses one observes two different regimes, one for low fluences and one for high fluences[23], as shown in figure 15 (the figure is reprinted from the website of the NCLA in Ireland[25]). The logarithmic law (2) can be rewritten as:

$$z_{abl,1,2} = \delta_{1,2} \cdot \ln\left(\frac{\phi}{\phi_{th,1,2}}\right)$$

With two penetration depths $\delta_{1,2}$ and threshold fluences $\phi_{1,2}$ for the first and the second regime, respectively.

The blue line in figure 16 denotes the ablation depth as a function of the fluence for ϕ_{th} = 1J/cm^2 and δ = 500nm. One can ask for the difference between one pulse with energy E_P and fluence ϕ_p or n pulses with energy E_P/n and fluence ϕ_p/n. Under the assumption that in the case of multiple pulses the result of each pulse is not influenced by the leading pulse, the ablation depth is given by:

$$z_{abl}(n) = n \cdot \delta \cdot \ln\left(\frac{\phi_{tot}/n}{\phi_{th}}\right) \tag{3}$$

The result for a fluence (n = 1) of 10J/cm^2 is shown with red dots in figure 16, where a clear optimum with maximum ablation depth exist for n = 4. A short calculation leads to:

$$n_{\max} = \frac{1}{e} \cdot \frac{\phi_{tot}}{\phi_{th}} \quad \text{and} \quad z_{abl,\max} = \frac{1}{e} \cdot \delta \cdot \frac{\phi_{tot}}{\phi_{th}} \tag{4}$$

It is noted, that n_{max} does not automatically correspond to a nonnegative integer.

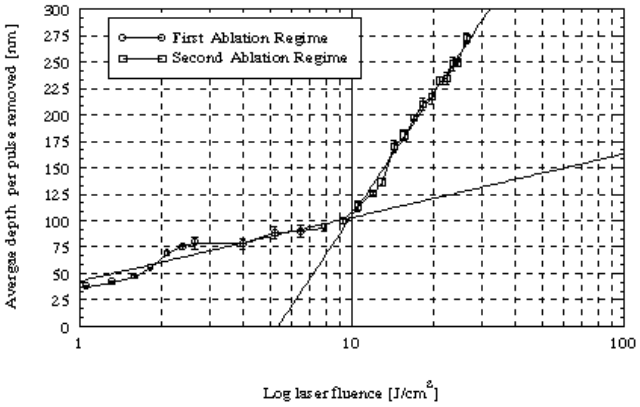

Figure 15: Ablation depth as a function of the laser fluence for steel[25]. The pulse duration was 150fs.

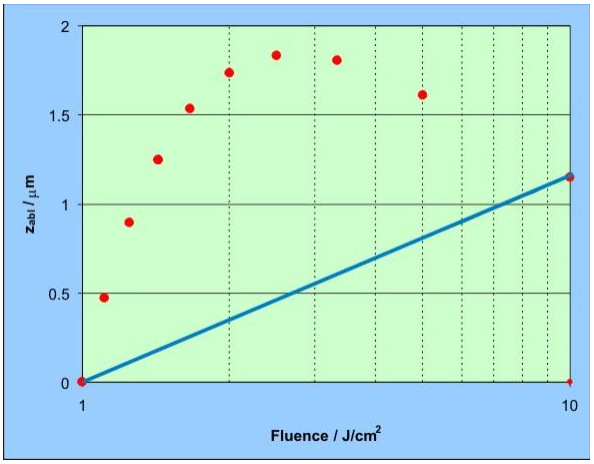

Figure 16: Ablation curve (blue) for $\phi_{th} = 1J/cm^2$ and $\delta = 500nm$ and the ablation depth when corresponding to (4) for a total fluence of $10J/cm^2$.

The process efficiency is not given by the ablation depth but by the ablated volume per time. For a top hat intensity profile of radius w_0 the ablated depth can be simply calculated by (2):

$$z_{abl}(r) = \begin{cases} \delta \cdot \ln\left(\frac{\phi}{\phi_{th}}\right) & r \le w_0 \\ 0 & r > w_0 \end{cases} \tag{5}$$

For a Gaussian beam of radius w_0 this depth as a function of the distance r to the center of the beam reads:

$$z_{abl}(r) = \begin{cases} \delta \cdot \left(\ln\left(\frac{\phi_0}{\phi_{th}}\right) - 2 \cdot \frac{r^2}{w_0^2} \right) & r \le R \\ 0 & r > R \end{cases} \quad \text{with:} \quad R = \frac{w_0}{\sqrt{2}} \cdot \sqrt{\frac{\phi_0}{\phi_{th}}} \quad \text{and} \quad \phi_0 = \frac{2 \cdot E_p}{\pi \cdot w_0^2} \tag{6}$$

Where ϕ_0 denotes the peak fluence in case of a Gaussian beam. From (5) and (6) the ablated volume per pulse ΔV can be calculated. After a short calculation one obtains for a top hat profile:

$$\Delta V = \pi \cdot w_0^2 \cdot \delta \cdot \ln\left(\frac{\phi}{\phi_{th}}\right) \tag{7}$$

and for a Gaussian beam:

$$\Delta V = \frac{1}{4} \cdot \pi \cdot \delta \cdot w_0^2 \cdot \ln^2\left(\frac{\phi_0}{\phi_{th}}\right) \tag{8}$$

5.2 Expansion of the model to constant average power

Modern ultra short pulsed systems do mostly not significantly vary in the average power when the repetition rate is changed. Case of simplicity a constant average power is assumed for the following considerations. At a fixed average power P and spot radius w_0 the pulse energy, the fuence ϕ and the peak fluence ϕ_0 (in case of a Gaussian beam) depend on the repetition rate f:

$$E_p = \frac{P}{f}, \quad \phi = \frac{P}{f \cdot \pi \cdot w_0^2}, \quad \phi_0 = \frac{2 \cdot P}{f \cdot \pi \cdot w_0^2} \tag{9}$$

The total ablated volume per time $\dot{V}$, the volume ablation rate, is given by:

$$\dot{V} = f \cdot \Delta V \tag{10}$$

Introducing (9) into (7)/(8) and this into (10) final leads to:

$$\dot{V} = \pi \cdot w_0^2 \cdot \delta \cdot f \cdot \ln\left(\frac{P}{f \cdot \pi \cdot w_0^2 \cdot \phi_{th}}\right) \tag{11}$$

for a top hat beam and

$$\dot{V} = \frac{1}{4} \cdot \pi \cdot w_0^2 \cdot \delta \cdot f \cdot \ln^2\left(\frac{2 \cdot P}{f \cdot \pi \cdot w_0^2 \cdot \phi_{th}}\right) \tag{12}$$

for a Gaussian beam. In both cases it can clearly be seen, that the volume ablation rate depends on the repetition rate at a given average power. Figure 17 shows these results for an average power of 10W, a spot radius of 7.5µm, a threshold fluence of 1J/cm^2 and a penetration depth of 500nm. It is obvious, that a maximum volume ablation rate can be achieved at a optimum repetition rate. Beyond and below this repetition rate the volume ablation rate significantly drops down. A top hat intensity distribution would be more efficient than a Gaussian beam. This is clear when one considers that all the energy in the wings of a Gaussian beam below the threshold fluence is lost.

In the case of a top hat beam this maximum volume ablation rate and optimum repetition rate are given by:

$$f_{opt} = \frac{1}{e} \cdot \frac{P}{\pi \cdot w_0^2 \cdot \phi_{th}} \quad \text{and} \quad \dot{V}_{\max} = \frac{\delta}{e} \cdot \frac{P}{\phi_{th}} \tag{13}$$

And for a Gaussian beam follows:

$$f_{opt} = \frac{1}{e^2} \cdot \frac{2 \cdot P}{\pi \cdot w_0^2 \cdot \phi_{th}} \quad \text{and} \quad \dot{V}_{\max} = 2 \cdot \frac{\delta}{e^2} \cdot \frac{P}{\phi_{th}} \tag{14}$$

From both, (13) and (14) follows that the maximum volume ablation rate linearly scales with the average power, but only at the optimum repetition rate. In the case of 2 regimes (2b) one has to make the calculations (13) or (14) for both regimes and to compare the results. In most cases the optimum values lies in the first regime. Also an exact calculation of the ablated Volume per pulse for a Gaussian beam with the results of figure 15 shows that the optimum lies in the first regime.

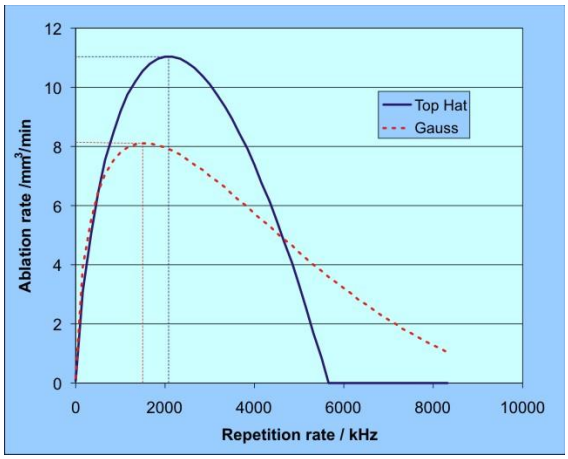

Figure 17: Calculated volume ablation rate as a function of the repetition rate for an average power of 10W, a spot radius of 7.5µm, a threshold fluence of 1J/cm^2 and a penetration depth of 500nm.

To confirm this model a series of lines at the wavelength 1064nm were written into a polished copper surface. The average power was kept at 3W and the repetition rate was varied between 25kHz and 300kHz. The lines were written with a constant pulse overlap by adapting the marking speed. The results are summarized in figure 18 where a very good agreement between the measured values and the model (12) can be observed. The fit of the model to the data leads to ϕ_{th} = 1.07J/cm^2 and δ = 33nm. The existence of an optimal repetition rate was also confirmed in other works[25].

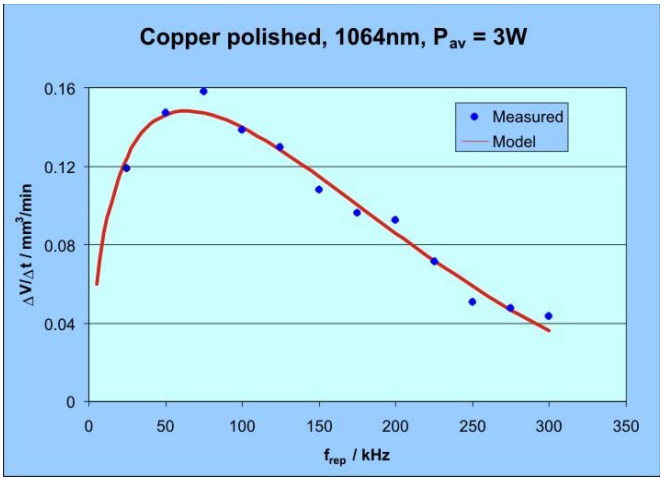

Figure 18: Calculated volume ablation rate as a function of the repetition rate for an average power of 10W, a spot radius of 7.5µm, a threshold fluence of 1J/cm^2 and a penetration depth of 500nm.

5.3 Consequences from the model

When the results from the previous section are extrapolated to an average power of 50W, a maximum volume ablation rate of 3.4mm^3/min for a top hat beam (13) and 2.54mm^3/min for a Gaussian beam (14) would be achieved. The optimum repetition rate strongly depends on the spot radius.

For a top hat distribution with radius 25µm, generated e.g. with a pi-shaper, this optimum repetition rate amounts about 870kHz. When a strategy as presented in 4 should be used, the marking speed would be about 22m/s.

For structures with lateral dimensions of about 100µm the diameter of a Gaussian beam should not exceed 15µm. In this case the optimum repetition rate becomes 7.1MHz and the marking speed has to be about 100m/s when the distance from pulse to pulse should be in the range of one beam diameter.

Both short calculations show that there are huge demands for the beam guiding system. Another critical point would be the missing opportunities to pick single pulses at repetition rates far above 1MHz. Today, no beam guiding technology

exists, which can guarantee the desired accuracy at such high marking speeds i.e. the average power of today ps-laser systems can't fully be used for 3d-micro structuring.

6. CONCLUSIONS

Laserpulses with durations in the range of 10ps are very well suited for micro processing of metals, dielectric materials and semiconductors. In metals they benefit from the electron-phonon thermalization time which lies in the same range. For transparent dielectric materials the induced nonlinear effects are strong enough to facilitate direct processing with wavelengths in the visible or near UV range. For the removal of thin films in solar cells industries ps-pulses are often the only way to achieve the desired quality and accuracy at industrial reasonable efforts and costs. With different strategies ps laserpulses can be ideally used for 3d structuring of almost any surfaces. For structures with lateral dimension of several 100µm up to a few mm galvo scanners can be used. For smaller structures a strategy where one slice is divided into different layers is very promising. For this, today galvo scanner can't fulfill the requirements with respect to accuracy and control of the instant position.

A simple model based on the logarithmic ablation law clearly shows, that a maximum volume ablation rate can be obtained at an optimum repetition rate for a fixed average power. This maximum volume ablation rate and the optimum repetition rate linearly depend on the average power and lie in the range of several mm^3/min and a few *MHz* for an average power of 50W and a spot radius of about 15µm. The corresponding marking speeds amount about 100m/s. With beam conversion optics like a pi-shaper or a Gauss to top hat converter the optimum repetition rate can be reduced to several 100 *kHz* but beam guiding rests still a problem.

For 3d structuring there is a great lack in beam guiding systems to really take benefit of high average powers which are essential for an economical reasonable industrial use of ps laser systems. The development of future ps-systems goes towards several 100W of average power i.e. future beam guiding systems have to enable marking speeds in the range of several 100m/s. Additionally only a precise control of the position where a pulse impinges on the surface opens the way to optimized strategies for very small structures with low surface roughness. New beam guiding and control concepts have therefore to be developed in near future to leverage this technology in the industrial field.

REFERENCES

1. B.N. Chichov, C. Momma, S. Nolte, F. van Alvensleben and A. Tünnermann, "Femtosecond, picosecond and nanosecond laser ablation of solids", Applied Physics A, 63, 109-115 (1996)
2. Friedrich Dausinger, Helmut Hügel and Vitali Konov, "Micro-machining with ultrashort laser pulses: From basic understanding to technical applications", Proc. SPIE, 5147, 106-115 (2003)
3. Detlef Breitling, Andreas Ruf and Friedrich Dausinger, "Fundamental aspects in machining of metals with short and ulrashort laser pulses", Proc. SPIE 5339, 49-63 (2004)
4. Time Bandiwth Products AG, http://www.tbwp.com/index.html
5. Lumera, http://www.lumera-laser.com/index.php?id=98
6. V.V. Agadjanov, "Method of marking decorative articles", SU321422 (1972)
7. J. Zhang, K. Sugioka and K. Midorikava, "Laser-induced plasma-assisted ablation of fused quartz using the fourth harmonic of a Nd^+:YAG laser", Appl. Phys. A, 67, 545-549 (1998)
8. Jie Zhang, Koji Sugioka and Katsumi Midorikawa, "Direct fabrication of micrograting in fused quartz by laser-induced plasma-assisted ablation with KrF excimer laser", Opt. Letters, Vol 23. No. 18, September 15, 1486-1488 (1998)
9. J. Zhang, K. Sugioka and K. Midorikawa, "High-speed machining of glass materials by laser-induced plasma-assisted ablation using a 532-nm laser", Appl. Phys. A, 67, 499-501 (1998)
10. J. Zhang, K. Sugioka and K. Midorikawa, "High-Quality and high-efficiency machining of glass materials by laser-induced plasma-assisted ablation using conventional nanosecond UV, visible, and infrared lasers", Appl. Phys. A, 69, 879-882 (1999)
11. Y. Hanada, K. Sugioka, I. Miyamoto and K. Midorikawa, "LIPAA technique and its possible impact on micro-electronics", Proc. SPIE 5713, 445-455 (2005)
12. Y. Hanada, K. Sugioka and K. Midorikawa, "Laser-induced plasma-assisted ablation (LIPAA): fundamental and industrial applications", Proc. SPIE 6261, Paper 626111 (2006)

13. B. Neuenschwander et all, “Direct generation of conducting microstructures by laser induced plasma assisted ablation with ps laserpulses” Proceedings of the fifth international WLT conference on lasers in manufacturing 2009, 819 – 824
14. S. Lauzurica, et al, “Comparitive study on nanosecond and picoseconds laser patterning of thin film for photovoltaic solar moduls based on a-Si:H”, Proceedings of the fifth international WLT conference on lasers in manufacturing 2009, 635 – 640
15. M. Colina et al, “Micro-ramann study of the thermal affected zone generated after a laser scribing process in a-Si:H photovoltaic thin films”, Proceedings of the fifth international WLT conference on lasers in manufacturing 2009, 641 – 645
16. H.P. Huber et al, “Structuring of CIS thin-film solar cells by ultrafast laser pulses with industrial relevant process speed”, Proceedings of the fifth international WLT conference on lasers in manufacturing 2009, Postdeadline paper
17. C. Hartmann et al, “Investigation on laser micro ablation of metals using ns-multipulses”, Journal of Physics: Conference Series, 59, 440-444 (2007)
18. C. Hartmann and A. Gillner, “Investigation on laser micro ablation of steel using ps-IR pulse bursts”, *LIA Conference Proceedings 2007*, LIA, Orlando, 38–44 (2007)
19. http://www.swisslaser.net/libraries.files/Gillner_Vortrag-Ultrakurzpulslaser-Gillner1.pdf
20. G. Hennig, K-H. Selbmann, J. Brendel, S. Brüning, P. Dietiker and B. Neuenschwander, „Laserstrukturierung grossflächiger Tiefdruckwalzen mit Mikropräzision“, Tagungsband Laser in der Elektronikproduktion & Feinwerktechnik (2009)
21. M. Hashida et al, „Ablation threshold dependence on pulse duration for copper“, applied surface science, 197-198, pp. 862-867 (2002)
22. P. Mannion, J. Magee, E. Coyne and G.M. O’Conner, „Ablation thresholds in ultrafast laser micro-machining of common metals in air”, Proc. SPIE 4876, 470 – 478 (2003)
23. R. Le Harzic et al, “Pulse width and energy influence on laser micromachining of metals in a range of 100fs to 5ps”, applied surface science, 249, 322 – 331 (2005)
24. http://www.ncla.ie/apps_ultrafast_apps.htm
25. H. Pantsar, P. Laakso, R. Penttilä; “Material removal rates of metals using UV and IR picosecond pulses”, Proceedings of the Fourth International WLT-Conference on Lasers in Manufacturing 2007, 613 – 618